UDC 551.515.21:551.509.313

A NUMERICAL MODEL OF THE SLOWLY VARYING TROPICAL CYCLONE IN ISENTROPIC COORDINATES

RICHARD A. ANTHES

National Hurricane Research Laboratory, Environmental Research Laboratories, NOAA, Miami, Fla.

ABSTRACT

A diagnostic axisymmetric model in isentropic coordinates is developed to study the effect of differential heating on the dynamics and energetics of the steady-state tropical cyclone. From the thermal forcing specified by various heating distributions, slowly varying solutions for the mass and momentum fields are obtained by an iterative technique.

The theory of available potential energy for open systems is utilized to study the energy budget for the hurricane. In the slowly varying state, the gain of available potential energy by diabatic heating and lateral boundary processes balances the conversion of potential to kinetic energy that, in turn, offsets frictional dissipation. For a domain of radius 500 km, the boundary flux of available potential energy is about 40 percent of the generation by diabatic heating. For a domain of radius 1000 km, however, the boundary flux is about 15 percent of the generation.

Horizontal and vertical mixing are studied through the use of constant exchange coefficients. As the horizontal mixing decreases, the maximum surface wind increases and moves closer to the center.

Several horizontal and two vertical distributions of latent heating are investigated. The maximum surface wind is dependent primarily on heating within 100 km. The transverse (radial) circulation is closely related to the heat release beyond 100 km. In experiments in which the vertical variation of heating is pseudoadiabatic, the temperature and outflow structures are unrealistic. A vertical distribution that releases a higher proportion of heat in the upper troposphere yields results that are more representative of the hurricane.

CONTENTS

1. INTRODUCTION

Within the last decade, numerical modeling has become a powerful tool for investigating the life cycle of tropical cyclones. With a realistic parameterization of latent heat release, the models of Yamasaki (1968*a*, 1968*b*), Ooyama (1969), and Rosenthal (1969) have been successful in duplicating many observed features of tropical storms. The practical limitations of computer size and speed, however, have so far restricted these models (and also the present model) to two dimensions.

In the parameterization of the heat imparted to the environment by the cumulus convection by Kuo (1965), Rosenthal (1969), and others, large-scale heating is a function of the cloud-environment temperature difference and the net moisture convergence in a column. These models release a much larger proportion of heat in the upper troposphere than the heat released by earlier models based on a pseudoadiabatic process.

The importance of latent heat release within the warm core for the production of kinetic energy was recognized by Palmén (1948) and re-emphasized by Yanai (1964). In simplest terms, the release of latent heat maintains the baroclinicity that drives the transverse radial circulation. The horizontal kinetic energy is produced in both the inward- and outward-flowing branches by accelerations toward lower pressure. This production of kinetic energy, in turn, offsets surface and internal frictional dissipation.

The conversion of potential to kinetic energy through cross-isobar flow has been examined in several diagnostic studies (e.g., Palmén and Jordan 1955, Palmén and Riehl 1957, Riehl and Malkus 1961, Miller 1958, and Hawkins and Rubsam 1968). Recently, Anthes and Johnson (1968) estimated the generation of available potential energy by diabatic heating in hurricane Hilda, 1964, and concluded that the generation within a 1000-km region was sufficient to balance the conversion to kinetic energy. Thus, on this scale, it was possible to consider that the hurricane was a self-sustaining system.

The importance of differential heating and cooling is emphasized in the theory of available potential energy. The sensitivity of the generation to different horizontal and vertical distributions of heating in Anthes and

Johnson's (1968) results suggests investigating the effect of differential heating on the dynamics as well as the energetics of tropical storms. In particular, the relation between generation of available energy and conversion to kinetic energy within the storm system should be studied to clarify the role of thermal versus mechanical forcing. This relationship has important implications in storm modification experiments in which the heating, generation, and possibly the conversion are altered in some manner.

Although interactions between temperature and momentum structure and large-scale heating certainly exist, the hurricane may be considered a direct consequence of thermal forcing. It makes sense, therefore, to study the response of the hurricane to differential heating by specifying steady heating distributions. The mass and momentum fields that develop in response to the steady forcing functions are useful in interpreting transient stages of hurricane forecast models as well as in testing various heating parameterizations.

The dynamics and energetics of the hurricane's response to thermal forcing are studied through a two-dimensional model in isentropic coordinates. An iterative technique is utilized to obtain slowly varying solutions of mass and momentum for different vertical and horizontal latent heating distributions and sensible heat addition at the earth's interface. The effects of vertical and horizontal mixing are also considered.

The present model differs from previous axisymmetric hurricane models in the following respects:

1. Only the slowly varying solutions for the mass and momentum fields that correspond to the mature hurricane are considered.
2. In contrast to previous steady-state models, the mass and momentum fields are investigated as functions of applied thermal forcing rather than vice versa. These experiments are numerical analogs to laboratory dishpan experiments that study fluid dynamics as a function of fixed heating (cooling) rates. The direct response of hurricane *dynamics* to variations in *heating* are relevant in view of the current interest in storm modification.
3. Isentropic coordinates are utilized for the first time in a system that includes diabatic effects. The results may therefore be of interest in areas outside the hurricane modeling problem.
4. The recent theory (exact in isentropic coordinates) of the available potential energy of open, isolated storm systems (Johnson 1970) is applied to the complete hurricane system.

2. AVAILABLE POTENTIAL ENERGY OF LIMITED REGIONS

The theory of available potential energy has historically been applied to the entire atmospheric system (Margules 1905, Lorenz 1955, and Dutton and Johnson 1967). Recently, however, Johnson (1970) has developed the theory for an open system to define the available potential energy of a storm and its time rate of change.

One appealing aspect of applying the theory of available potential energy to a tropical cyclone is the condition that, as a first approximation, the hurricane may be considered an isolated baroclinic disturbance superimposed on the nearly flat and horizontal barotropic Tropics. Thus one might reasonably expect the available potential energy generated on the tropical cyclone scale to be converted to kinetic energy within the same scale. This may not be true in the middle latitudes where the flux of energy across the boundaries of systems will be large.

Symbols used frequently in this work are:

A	available potential energy,
C_D	drag coefficient,
c_p	specific heat at constant pressure,
f	Coriolis parameter,
g	acceleration of gravity,
i, I	vertical grid index, maximum index,
j, J	horizontal grid index, maximum index,
k	specific kinetic energy$=(1/2)(v_\lambda^2+v_r^2)$,
K	total kinetic energy,
K_H	horizontal coefficient of eddy viscosity,
K_T	horizontal coefficient of thermal diffusion,
K_z	vertical coefficient of eddy viscosity,
p	pressure,
p_0	reference pressure$=1000$ mb,
$\dot{Q}$	heating rate per unit mass,
q_s	saturation specific humidity,
R	maximum radial distance of domain,
R_d	gas constant of dry air,
r	radial distance,
Δr	horizontal grid increment,
T	absolute temperature,
T_s	moist-adiabatic temperature,
Δt	time (iteration) step,
$\mathbf{V}$	horizontal wind vector,
v_λ	tangential wind component,
v_r	radial wind component,
z	height,
Δz	depth of boundary layer (assumed constant),
θ	potential temperature,
θ_e	equivalent potential temperature,
θ_0	coldest θ in domain,
θ_t	top isentropic surface in model,
$\Delta\theta$	vertical grid increment,
κ	R_d/c_p,
λ	tangential direction,
ρ	air density,
σ	area,
ψ	Montgomery potential$=c_pT+gz$,
$(\ )_r$	subscript r denoting reference atmosphere,
$(\ )_s$	subscript s denoting surface, $z=0$,
$\overline{(\ )}$	operator denoting area average,
∇_θ	del operator on isentropic surface,
∇^2	operator$=\partial^2/\partial r^2+(1/r)(\partial/\partial r)$, and
θ_B	vertical (upper or lower) boundary.

A. AVAILABLE POTENTIAL ENERGY EQUATIONS FOR THE MODEL

When one follows Johnson (1970), the available potential energy, A, of any region in hydrostatic balance is

$$A=\frac{c_p}{p_0^\kappa g(1+\kappa)}\int_\sigma\int_0^\infty(p^{1+\kappa}-p_r^{1+\kappa})d\theta d\sigma. \qquad (1)$$

When one divides the vertical integration into three parts, eq (1) becomes

$$A=\frac{c_p}{p_0^{\kappa}g(1+\kappa)}\int_\sigma\left[\int_0^{\theta_0}(p^{1+\kappa}-p_r^{1+\kappa})d\theta + \int_{\theta_0}^{\theta_t}(p^{1+\kappa}-p_r^{1+\kappa})d\theta+\int_{\theta_t}^{\infty}(p^{1+\kappa}-p_r^{1+\kappa})d\theta\right]d\sigma. \quad (2)$$

In eq (2), θ_0 is the lowest potential temperature in the region; and θ_t is the isentropic surface above which the atmosphere is assumed to be barotropic. The third integral vanishes by the barotropic assumption. When one follows Lorenz' convention that the pressure on isentropes which intersect the ground equals the surface pressure, the available potential energy for the model is

$$A=\frac{c_p}{p_0^{\kappa}g(1+\kappa)}\left[\theta_0\int_\sigma(p_s^{1+\kappa}-\bar{p}_s^{1+\kappa})d\sigma + \int_\sigma\int_{\theta_0}^{\theta_t}(p^{1+\kappa}-\bar{p}^{1+\kappa})d\theta d\sigma\right]. \quad (3)$$

In eq (3), we have used the conditions that, for hydrostatic atmospheres,

$$p_r(\theta)=\bar{p}(\theta) \text{ and } p_{s_r}=\bar{p}_s.$$

In this model in which heating vanishes on the upper boundary, the time rate of change of A is

$$\frac{dA}{dt}=\mathrm{G}+\mathrm{C}+\mathrm{B} \quad (4)$$

where

$$\mathrm{G}=-\frac{1}{g}\int_\sigma\int_{\theta_0}^{\theta_t}[1-(\bar{p}/p)^{\kappa}]\dot{Q}\frac{\partial p}{\partial\theta}d\theta d\sigma, \quad (5)$$

$$\mathrm{C}=-\frac{1}{g}\int_\sigma\int_{\theta_0}^{\theta_t}(V\cdot\nabla_\theta\psi)\frac{\partial p}{\partial\theta}d\theta d\sigma, \quad (6)$$

and

$$\mathrm{B}=\frac{1}{g}\int_\sigma\int_{\theta_0}^{\theta_t}\nabla_\theta\cdot\frac{\partial p}{\partial\theta}(\psi-\psi_r)Vd\theta d\sigma. \quad (7)$$

The generation, G, by diabatic heating is positive for heating at high pressure and cooling at low pressure. The conversion, C, is the production of kinetic energy by cross-isobar flow. The last term, B, represents the change of A by mass flux across the lateral boundary. For the axisymmetric model, B simplifies to

$$\mathrm{B}=\frac{2\pi R}{g}\int_{\theta_0}^{\theta_t}v_r(\psi-\psi_r)\frac{\partial p}{\partial\theta}d\theta. \quad (8)$$

For the hurricane, the surface pressure at the outer boundary will be greater than the mean surface pressure, so that $\psi>\psi_r$. From the low-level inflow, the covariance of $(\partial p/\partial\theta)(v_r)$ and $(\psi-\psi_r)$ will be positive. In the outflow region, $(\psi-\psi_r)$ tends to vanish; thus the integral B usually provides a positive contribution to dA/dt.

B. BUDGET EQUATIONS FOR VOLUME

In this subsection, the time-dependent budget equations are summarized for a stationary cylindrical volume. If f is any specific quantity, such as water vapor per unit mass, the total amount of the property in the volume is

$$F=\int_0^{2\pi}\int_0^R\int_{\theta_0}^{\theta_t}r\rho\frac{\partial z}{\partial\theta}fd\theta dr d\lambda. \quad (9)$$

With the aid of Leibnitz' rule, the hydrostatic assumptions, and the continuity equation, the time rate of change of F (Johnson 1970) is

$$\frac{dF}{dt}=-\frac{1}{g}\int_0^{2\pi}\int_0^R\int_{\theta_0}^{\theta_t}\left[\frac{\partial}{\partial t}\left(rf\frac{\partial p}{\partial\theta}\right)+\frac{\partial}{\partial\lambda}\left(rf\frac{\partial p}{\partial\theta}\frac{d\lambda_B}{dt}\right) + \frac{\partial}{\partial r}\left(rf\frac{\partial p}{\partial\theta}\frac{dR}{dt}\right)+\frac{\partial}{\partial\theta}\left(rf\frac{\partial p}{\partial\theta}\frac{d\theta_B}{dt}\right)\right]d\theta dr d\lambda. \quad (10)$$

Equation (10) is greatly simplified for the stationary axisymmetric volume of this study in which all tangential derivatives vanish and $dr_B/dt=0$. With these conditions and the use of the continuity equation,

$$\frac{dF}{dt}=-\frac{2\pi}{g}\int_0^R\int_{\theta_0}^{\theta_t}\left(-\frac{\partial}{\partial r}\left(rfv_r\frac{\partial p}{\partial\theta}\right) -\frac{\partial}{\partial\theta}\left(rf\frac{\partial p}{\partial\theta}\left(\frac{d\theta}{dt}-\frac{d\theta_B}{dt}\right)\right)+r\frac{\partial p}{\partial\theta}\frac{df}{dt}\right)d\theta dr. \quad (11)$$

The upper and lower boundary conditions are

$$d\theta_B/dt=d\theta_s(r,\theta_s,t)/dt$$

and

$$d\theta_t/dt=d\theta_B/dt=0.$$

With these conditions and after integration, the final budget equation becomes

$$\frac{dF}{dt}=\frac{2\pi R}{g}\int_{\theta_0}^{\theta_t}\left(fv_r\frac{\partial p}{\partial\theta}\right)_R d\theta-\frac{2\pi}{g}\int_0^R\int_{\theta_0}^{\theta_t}r\frac{\partial p}{\partial\theta}\frac{df}{dt}d\theta dr. \quad (12)$$

The first term is the change of F caused by transport of f across the lateral boundary while the second term is the change due to sources or sinks within the volume. The generalized budget and available potential energy equations provide integrated parameters for the hurricane volume, which are studied as the mass and momentum fields seek steady-state conditions for the applied thermal forcing.

3. THE DIAGNOSTIC MODEL

One of the appealing aspects of numerical modeling in isentropic coordinates is the absence of a "vertical velocity" in the equations of motion for isentropic flows. Such a model should have less truncation error than models in pressure or height coordinates that must include vertical advection terms. Even under diabatic conditions, it is probable that the vertical truncation is less in isentropic coordinates because the adiabatic part of the vertical motion should be free of error.

Besides the reduction in vertical truncation error, there are several other possible advantages of modeling in

isentropic coordinates:

1. The theory of available potential energy is exact in isentropic coordinates (Dutton and Johnson 1967).
2. Johnson and Dutton (1969) stress that mean energy and momentum transport processes of the general circulation are explicitly coupled with thermal forcing.
3. Horizontal resolution and vertical resolution are higher in the energetically active baroclinic zones.

Difficulties in using isentropic coordinates arise chiefly near the ground where superadiabatic lapse rates are found and isentropic surfaces intersect the ground. The first problem generally arises over small areas and may be solved by utilizing height coordinates in the boundary layer and isentropic coordinates above. The second has been reasonably well resolved by an interpolation scheme in some preliminary adiabatic experiments by Eliassen and Raustein (1968).

To the author's knowledge, there has been no previous work with numerical modeling in isentropic coordinates that includes diabatic processes. In this particular series of experiments in which the heating function is specified and the steady-state response determined, isentropic coordinates are especially attractive because the form of the thermodynamic equation is greatly simplified. In a broader sense, the experience gained by studying thermal forcing in this model should be useful in future work with more advanced numerical models.

A. STEADY STATE OR SLOWLY VARYING CONCEPT

The term "steady state," when applied to the tropical cyclone, usually refers to the storm's mature stage in which certain significant parameters, such as central pressure and maximum wind, remain relatively unchanged over a period of time. The axisymmetric assumption is usually best satisfied during this mature stage. It is difficult, if not impossible, for an entire axisymmetric hurricane system to reach a steady state, particularly in the outflow layer at radii greater than 400 km from the storm center (Anthes 1970*b*). However, steady-state solutions that compare favorably with observations are possible near the center of the storm, even under the axisymmetric assumption (Krishnamurti 1961 and Barrientos 1964).

In the iteration technique used in this model, mass and momentum are "forecast" using a constant specified heating function until the inner region reaches a slowly varying state. True steady-state conditions are never determined because of the large amount of time required to reach such a state. In typical experiments, changes from initial conditions in response to the constant heating function are very large during the first few iterations as the mass and momentum fields attempt to adjust to the new forcing function. Later, however, rates of change are less. When this "slowly varying" state is reached (usually after about 1,600 iterations), differences in the results caused by experimental variation of physical processes or parameters are apparent.

B. DESCRIPTION OF THE MODEL

Basic equations. The tangential and radial equations of motion and the continuity equation in isentropic coordinates are

$$\frac{\partial rv_\lambda}{\partial t}=-v_r\frac{\partial rv_\lambda}{\partial r}+r\left[-fv_r-\frac{d\theta}{dt}\frac{\partial v_\lambda}{\partial\theta}+K_H\left(\nabla^2 v_\lambda-\frac{v_\lambda}{r^2}\right)+\frac{\partial}{\partial z}\left(K_z\frac{\partial v_\lambda}{\partial z}\right)\right], \quad (13)$$

$$\frac{\partial v_r}{\partial t}=-v_r\frac{\partial v_r}{\partial r}+fv_\lambda+\frac{v_\lambda^2}{r}-\frac{\partial\psi}{\partial r}-\frac{d\theta}{dt}\frac{\partial v_r}{\partial\theta}+K_H\left(\nabla^2 v_r-\frac{v_r}{r^2}\right)+\frac{\partial}{\partial z}\left(K_z\frac{\partial v_r}{\partial z}\right), \quad (14)$$

and

$$\frac{\partial}{\partial t}\left(\frac{\partial p}{\partial\theta}\right)=-\frac{1}{r}\frac{\partial}{\partial r}\left(rv_r\frac{\partial p}{\partial\theta}\right)-\frac{\partial}{\partial\theta}\left(\frac{d\theta}{dt}\frac{\partial p}{\partial\theta}\right) \quad (15)$$

where the horizontal and vertical mixing terms in eq (13) and (14) are expressed in height coordinates rather than the more complex transformed expressions for computational convenience. This approximation is justified from the relatively large uncertainty in the form of K_H and K_z.

The vertical velocity term in isentropic coordinates, $d\theta/dt$, is computed from

$$\frac{d\theta}{dt}=-\frac{1}{c_p}\frac{\theta}{T}\dot{Q}+K_T\left\{-\left(\frac{\partial p}{\partial\theta}\right)^{-1}\times\left[\frac{\partial^2 p}{\partial r^2}-\left(\frac{\partial p}{\partial\theta}\right)^{-1}\frac{\partial p}{\partial r}\left(2\frac{\partial^2 p}{\partial r\partial\theta}-\left(\frac{\partial p}{\partial\theta}\right)^{-1}\frac{\partial p}{\partial r}\frac{\partial^2 p}{\partial\theta^2}\right)\right]+\left(r\frac{\partial p}{\partial\theta}\right)^{-1}\frac{\partial p}{\partial r}\right\}+\frac{\partial}{\partial z}\left(K_z\frac{\partial\theta}{\partial z}\right) \quad (16)$$

where $\dot{Q}$ is the parameterized heating rate and is prescribed as a function of mass. The second term in eq (16) results from approximating the horizontal diffusion by $K_T\nabla^2\theta$ in pressure coordinates and transforming to isentropic coordinates. Again, the uncertainties in K_T outweigh the error in approximation.

The lowest prediction level for the velocity components corresponds to the center of a boundary layer of constant depth, Δz, in which a linear variation of stress with height is assumed and vertical advection is neglected. The surface stress is approximated by the quadratic stress law with the surface wind assumed equal to the wind at the center of the boundary layer. Similar one-level Ekman layers have been utilized in hurricane models (Ooyama 1969, Yamasaki 1968*a*, 1968*b*, and Rosenthal 1969). Under the above assumptions, the equations of motion for the lowest

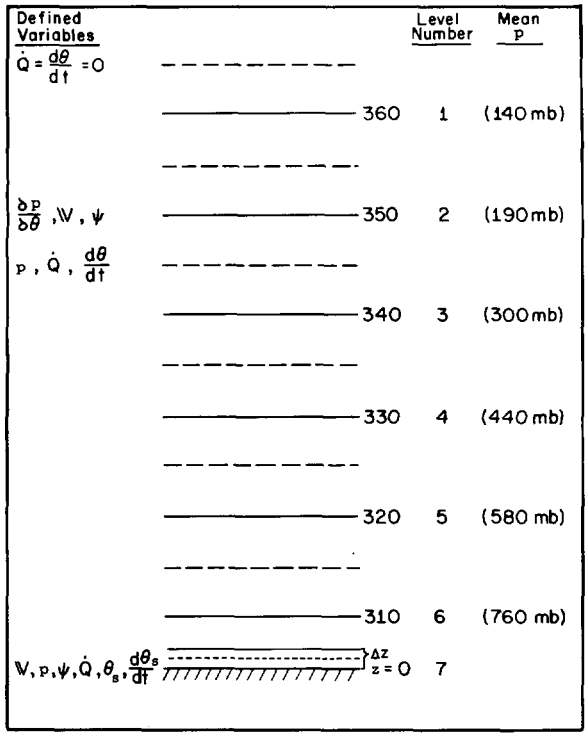

FIGURE 1.—Geometry of the isentropic model of the hurricane.

model level are

$$\frac{\partial rv_\lambda}{\partial t}=-v_r\frac{\partial rv_\lambda}{\partial r}+r\left[-fv_r-\frac{C_D|\mathbf{V}|v_\lambda}{\Delta z}+K_H\left(\nabla^2v_\lambda-\frac{v_\lambda}{r^2}\right)\right] \quad (17)$$

and

$$\frac{\partial v_r}{\partial t}=-v_r\frac{\partial v_r}{\partial r}+fv_\lambda+\frac{v_\lambda^2}{r}-\frac{c_p\theta}{p_0^\kappa}\frac{\partial p^\kappa}{\partial r}-\frac{C_D|\mathbf{V}|v_r}{\Delta z}+K_H\left(\nabla^2v_r-\frac{v_r}{r^2}\right). \quad (18)$$

The local change of surface potential temperature computed from the thermodynamic equation is

$$\frac{\partial\theta_s}{\partial t}=-v_r\frac{\partial\theta_s}{\partial r}+\frac{d\theta_s}{dt}+K_T\nabla^2\theta_s. \quad (19)$$

The remaining equations constituting the complete set are the hydrostatic equation

$$\frac{\partial\psi}{\partial\theta}=c_p\frac{T}{\theta} \quad (20)$$

and the definition of potential temperature

$$\theta=T(p_0/p)^\kappa. \quad (21)$$

Finite-difference equations. The geometry of the model (fig. 1) consists of six equally spaced isentropic surfaces ($\theta_i=370°\text{K}-i\Delta\theta$, $\Delta\theta=10°\text{K}$, $i=1,6$) and the sea-level surface. The approximate mean tropical pressures of the integer isentropic surfaces are given for reference (Jordan 1958). All variables are defined on the sea-level surface. On the isentropic surfaces, the variables are staggered for computational convenience with $\mathbf{V}$, ψ, and $\partial p/\partial\theta$ defined on integer surfaces. The horizontal grid is also staggered with $\mathbf{V}$ defined at $r=(j-1)\Delta r$ and the thermodynamic variables (ψ, p, $\dot{Q}$, $d\theta/dt$) defined at $r=(j-1/2)\Delta r$ for $j=1, 2, \ldots, J$. The horizontal domain extends to the radius R_j, which is either 500 or 1000 km.

In eq (13) through (19), all space derivatives are estimated by centered differences. The finite-difference form of eq (18) is given with the i index suppressed for simplicity:

$$\frac{\partial v_{r_j}}{\partial t}=-v_{r_j}\left(\frac{v_{r_{j+1}}-v_{r_{j-1}}}{r_{j+1}-r_{j-1}}\right)+fv_{\lambda_j}+\frac{v_{\lambda_j}^2}{r_j}$$
$$\times\frac{c_p\theta}{p_0^\kappa}\left(\frac{p_{j+3/2}^\kappa-p_{j+1/2}^\kappa}{r_{j+3/2}-r_{j+1/2}}\right)-\frac{C_D[v_{\lambda_j}^2+v_{r_j}^2]^{1/2}v_{r_j}}{\Delta z}$$
$$+K_H\left\{\frac{\frac{v_{r_{j+1}}-v_{r_j}}{r_{j+1}-r_j}-\frac{v_{r_j}-v_{r_{j-1}}}{r_j-r_{j-1}}}{0.5(r_{j+1}-r_{j-1})}-\frac{v_{r_{j+1}}-v_{r_{j-1}}}{r_j(r_{j+1}-r_{j-1})}-\frac{v_{r_j}}{r_j^2}\right\}. \quad (22)$$

The finite-difference approximation of the vertical mixing term is

$$\frac{\partial}{\partial z}\left(K_z\frac{\partial v_r}{\partial z}\right)_i\approx\frac{K_{z_{i-1}}\left(\frac{v_{r_{i-1}}-v_{r_i}}{z_{i-1}-z_i}\right)-K_{z_i}\left(\frac{v_{r_i}-v_{r_{i+1}}}{z_i-z_{i+1}}\right)}{0.5(z_{i-1}-z_i)}. \quad (23)$$

The unwieldy expressions for the second derivative terms are greatly simplified for a constant grid interval. The general form is retained, however, in anticipation of the use of a variable grid in some experiments.

The pressure is obtained from $\partial p/\partial\theta$ by integrating downward from a fixed value of p (365°K):

$$p_{i+1/2}=p_{i-1/2}-\left(\theta_{i-1/2}-\theta_{i+1/2}\right)\frac{\partial p}{\partial\theta_i}\qquad i=1, 2, \ldots, 5$$

and (24)

$$p_s=p_{11/2}-(\theta_{11/2}-\theta_s)\frac{\partial p}{\partial\theta_6}.$$

At the sea surface, θ_s equals $\theta_s(r)$. From an integration of the hydrostatic equation upward from sea level, ψ is

$$\psi_6=\psi_7+(\theta_6-\theta_s)c_p\left(\frac{\bar{p}}{p_0}\right)^\kappa$$

and

$$\psi_{i-1}=\psi_i+(\theta_{i-1}-\theta_i)c_p\left(\frac{p_{i-1/2}}{p_0}\right)^\kappa\qquad i=6, 5, \ldots, 2 \quad (25)$$

where

$$\bar{p}=p_s+\frac{1}{2}(\theta_6-\theta_s)\frac{\partial p}{\partial\theta_6}$$

and

$$\psi_7=c_pT_7.$$

Boundary conditions. Those for the top isentropic surface are $p=140$ mb, $d\theta/dt=0$, and $\partial V/\partial z=0$. At the lateral boundary, the pressure and temperature gradients, the horizontal divergence, and the relative vorticity are all assumed to vanish, which enables the calculation of the variables at R by

$$\begin{aligned} p_J&=p_{J-1},\\ (rv_r)_J&=(rv_r)_{J-1},\\ \psi_J&=\psi_{J-1},\\ (rv_\lambda)_J&=(rv_\lambda)_{J-1},\\ \text{and}\qquad (\theta_s)_J&=(\theta_s)_{J-1}. \end{aligned} \tag{26}$$

Computational procedure. The iteration technique to determine the steady-state solutions utilizes a simulated backward-difference scheme (Matsuno 1966), which has the desirable property of damping high-frequency waves. One cycle of the scheme is summarized with the superscript referring to the iteration step number:

1. Given values of v_λ^n, v_r^n, ψ^n, p^n, $(d\theta/dt)^n$, θ_s^n.
2. Forecast tentative values v_λ^*, v_r^*, $(\partial p/\partial\theta)^*$, θ_s^* at step $n+1$ (designated by an asterisk) using appropriate tendency eq (13) through (19) and values of variables at step n.
3. Calculate p^* and ψ^* using tentative estimates $(\partial p/\partial\theta)^*$ and θ_s^*.
4. Forecast final estimates of v_λ^{n+1}, v_r^{n+1}, $(\partial p/\partial\theta)^{n+1}$, and θ_s^{n+1} using * values of variables where they appear in tendency equations.
5. Calculate p^{n+1} and ψ^{n+1}.
6. Calculate $(d\theta/dt)^{n+1}$ from eq (16).
7. Calculate variables at the lateral boundary from eq (26). This completes one iteration step.

For determining when the quasi-steady state has been reached, the following norm on any iterated variable, f, is defined by

$$L_2\equiv\left[\frac{1}{N}\sum_{j=1}^{N}(f_j^n-f_j^{n-20})^2\right]^{1/2}. \tag{27}$$

After each 20th iteration cycle, L_2 is computed with f equal to the radial and tangential winds. The norm is computed for separate radial rings, 0–200, 200–400, 400–600 km, etc., and for each level to determine which parts of the domain reach a slowly varying state first.

Computational stability. The computational stability analysis of the complete set of equations is very complicated. Separate analyses were made for various combinations of the linearized prediction equations. The most stringent stability requirement from these results yields an estimate for the requirement for the complete set of nonlinear equations.

The most severe restriction on the size of the time increment, Δt, is governed by the speed of the external gravity wave (Anthes 1970*a*, appendix B). When one considers the continuity equation and the radial equation of motion, the criterion for linear computational stability is $(\Delta t/\Delta r)\sqrt{\bar{p}/\bar{\rho}}\leq 1$ where $\bar{\rho}$ and $\bar{p}$ are mean density and pressure, respectively, and $\sqrt{\bar{p}/\bar{\rho}}$ is the approximate speed of the external gravity wave (about 330 m/s).

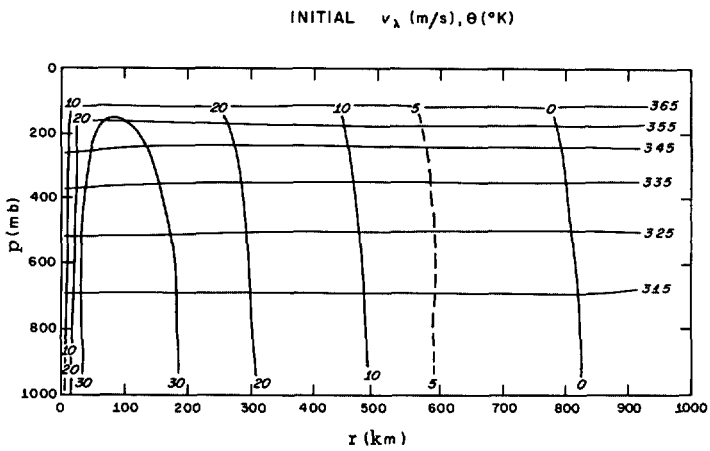

FIGURE 2.—Initial tangential wind and potential temperature cross section for all experiments.

Kinetic energy budget. The kinetic energy budget for the volume obtained by equating f to the specific kinetic energy, k, in eq (12) is

$$\frac{dK}{dt}=\frac{2\pi R}{g}\int_{\theta_0}^{\theta_t}\left(\frac{\partial p}{\partial\theta}kv_r\right)_R d\theta-\frac{2\pi}{g}\int_0^R\int_{\theta_0}^{\theta_t} r\frac{dk}{dt}\frac{\partial p}{\partial\theta}\,d\theta dr. \tag{28}$$

The time rate of change of the specific kinetic energy obtained by multiplying the tangential and radial equations of motion by v_λ and v_r, respectively, and adding becomes

$$\begin{aligned} \frac{dk}{dt}=&-v_r\frac{\partial\psi}{\partial r}+K_H\left[v_r\left(\nabla^2 v_r-\frac{v_r}{r^2}\right)+v_\lambda\left(\nabla^2 v_\lambda-\frac{v_\lambda}{r^2}\right)\right]\\ &+\frac{C_D}{\Delta z}|\mathbf{V}|(v_r^2+v_\lambda^2) && \text{surface only}\\ &+v_r\frac{\partial}{\partial z}\left(K_z\frac{\partial v_r}{\partial z}\right)+v_\lambda\frac{\partial}{\partial z}\left(K_z\frac{\partial v_\lambda}{\partial z}\right) && \theta \text{ levels only.} \end{aligned} \tag{29}$$

Initial conditions. In all experiments, the initial conditions (or first guess) consist of a vortex having tangential winds in gradient balance with a surface maximum of 37 m/s at 80 km (fig. 2), a weak warm core with a temperature excess of 1°C in the center, and a central pressure of 970 mb. Through the thermal wind relation, there is a slight decrease of wind speed with height. The environmental pressure is 1011 mb. The radial winds are calculated to balance the vertical divergence term in the continuity equation so that the initial pressure tendency is zero.

C. EXPERIMENTAL PARAMETERS

In the experiments presented in this paper, the constant parameters are the Coriolis parameter, the drag coefficient,

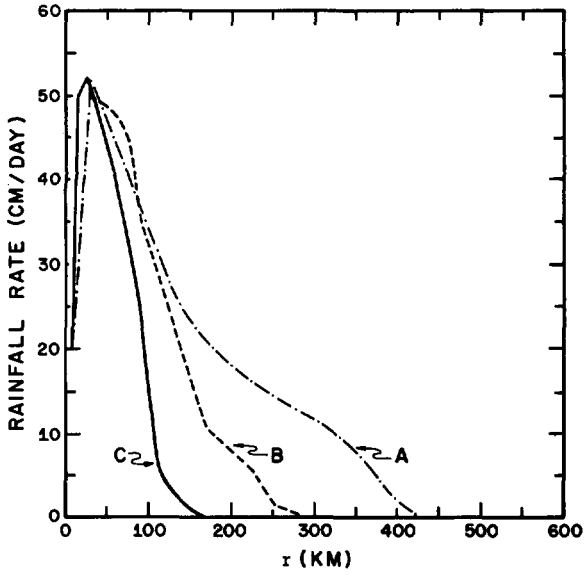

FIGURE 3.—Radial profiles of rainfall rates used to specify horizontal variations of latent heating.

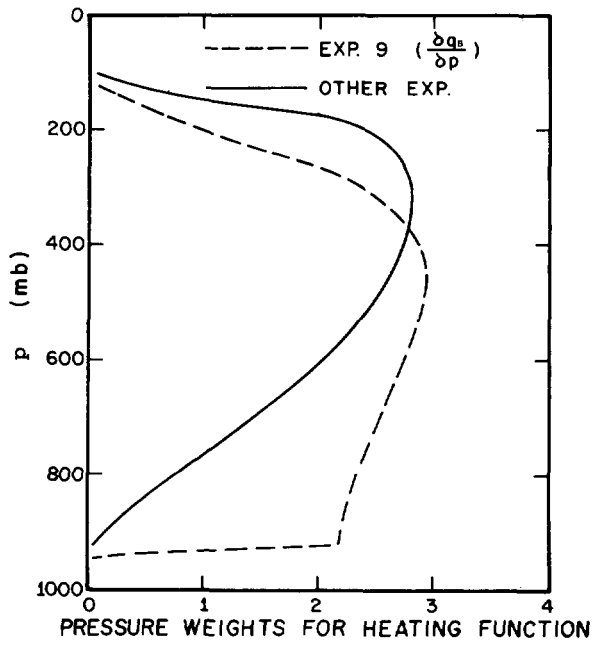

FIGURE 4.—Vertical profile of latent heat release for the experiments.

and the depth of the boundary layer. The Coriolis parameter is 5.0×10^{-5} s^{-1} and corresponds to 20°N. The drag coefficient, approximated by 0.003, is selected from empirical studies (Miller 1962). The depth of the boundary layer is assumed to be 1.0 km.

Very little is known about the variation of the vertical mixing coefficient, K_z. However, it seems qualitatively reasonable to assume that the vertical mixing decreases as the static stability increases. This effect is included in a crude fashion by decreasing K_z linearly with height from a value prescribed for the 315°K isentropic surface (about 700 mb) to one-half this value at the 365° surface. The value of K_z referred to in the experiments is the maximum value.

4. EXPERIMENTAL RESULTS

In this section, results from some preliminary experiments are presented. First, the role of internal (vertical and horizontal) mixing for a fixed heating function is investigated. Then for constant mixing coefficients, the response of the mass and momentum structures to various horizontal and vertical distributions of latent heating is studied. Later, the computational aspects of the model, such as domain size, resolution, and variable grid spacing, are considered; and finally, fine horizontal resolution is utilized to study the effects of reduced horizontal mixing.

In all experiments, the latent heating function is computed by arbitrarily assuming a radial profile of rainfall rates and distributing the equivalent amount of heat vertically. In figure 3, the rainfall rates that determine the horizontal heating distributions in the various experiments are presented. The maximum rainfall rate of 50 cm/day at 30 km (corresponding roughly to the eye wall) is quite moderate for a mature hurricane. For example, Riehl and Malkus (1961) estimate a rainfall rate of 90 cm/day in hurricane Daisy, 1958.

The variation of the vertical distribution is one of the interesting aspects of the problem in view of our lack of knowledge concerning the effective heat release for the hurricane scale. The two vertical profiles of latent heat release studied in the experiments are shown in figure 4. The basis for these profiles is discussed in subsection 4C. All experiments, except experiment 9, utilize the distribution that releases the higher proportion of heat in the upper troposphere.

The importance of sensible heating at the sea-air interface to hurricane development and maintenance has been established from both empirical (Malkus and Riehl 1960) and numerical (Ooyama 1969) results. As air flows inward toward lower pressure in the boundary layer, the sensible heating increases its equivalent potential temperature. The higher equivalent potential temperature enhances the convection and increases the heating and generation of available potential energy. In this model, however, there is no feedback between sensible and latent heating, and the model is insensitive to this effect. In computing $d\theta_s/dt$, eq (19) is approximated by

$$\frac{d\theta_s}{dt}=\frac{\theta_s}{c_pT_s}\dot{Q}_S\approx\frac{\dot{Q}_s}{c_p}. \tag{30}$$

The sensible heating, $\dot{Q}_s$, is modeled by assuming that the total sensible heating is 0.11×10^{14} W (Malkus and Riehl 1960) and distributing the heat radially, as shown in figure 5.

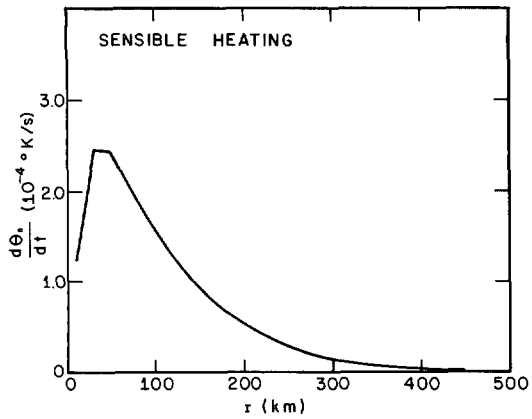

FIGURE 5.—Radial profiles of surface potential temperature change by sensible heating.

A. VARIATION OF INTERNAL MIXING

The proper formulation of internal mixing (both horizontal and vertical) is an important, but unfortunately poorly understood, aspect of numerical modeling. Because of the difficulty in making direct measurements, the dissipation of kinetic energy by internal mixing is usually estimated as a residual in empirical energy budgets (e.g., Riehl and Malkus 1961 and Hawkins and Rubsam 1968). These studies indicate that the kinetic energy dissipation by internal mixing is about the same magnitude as the dissipation at the surface.

The horizontal diffusion of momentum in the hurricane has been modeled using constant mixing coefficients, but the values used by different investigators (table 1) vary over several orders of magnitude. A further complication is that the truncation errors of the finite-difference schemes produce large nonlinear damping. It is therefore of interest to investigate the magnitude of explicit horizontal and vertical diffusion with a model that does not contain a large computational damping.

The vertical mixing process is even more complex than horizontal mixing because the vertical eddies (cumulus clouds) have the same vertical scale as the hurricane. Gray (1967) has found that the momentum transport by cumulus convection is an important process in the steady-state dynamics of hurricanes. Constant vertical mixing coefficients seem particularly inadequate to describe this process correctly. Indeed, Gray finds a large variation of the vertical mixing coefficients with height ranging from 10^6 to 10^9 cm^2/s.

Because of these uncertainties, the effects of horizontal and vertical mixing are investigated in experiments 1 through 6. The steady heating for these experiments is defined by the rainfall profile A (fig. 3) and the solid vertical profile in figure 4. The results from these preliminary experiments are discussed in some detail by Anthes (1970*a*), and only a brief summary is included here.

TABLE 1.—*Exchange coefficients (cm^2/s) in hurricanes*

Investigator	K_H	K_z	Remarks
Estoque and Fernandez-Partagas (1968)	10^8–10^9	-	Forecast model*
Gray (1967)	-	10^6–10^9	Empirical study
Kasahara (1961)	1.6×10^8	-	Forecast model*
Krishnamurti (1961)	2.7×10^9	1.2×10^7	Diagnostic study
Kuo (1965)	10^8	10^5–10^6	Forecast model
Ooyama (1969)	10^7	0-10^5	Forecast model
Riehl and Malkus (1961)	10^8	10^6	Empirical study
Rosenthal (1969)	10^8	0–10^5	Forecast model*
Yamasaki (1968*a*, 1968*b*)	10^7	10^5	Forecast model*

*Denotes additional nonlinear damping due to truncation error in finite-difference scheme

The results from experiments 1 through 6 establish ranges of the horizontal and vertical mixing coefficients that give results comparable to observations. Values of $K_H \geq 10 \times 10^8$ cm^2/s result in a large diffuse storm. Values of $K_z \leq 1 \times 10^6$ cm^2/s do not yield sufficient vertical mixing to produce the vertical momentum structure representative of hurricanes (Hawkins 1962, LaSeur and Hawkins 1963, Gray 1967, and Riehl and Malkus 1961). The strongest maximum wind and the results that compare most closely with the above empirical wind distributions (loc. cit.) are obtained for $K_H = 5 \times 10^8$ cm^2/s and $K_z = 5 \times 10^6$ cm^2/s; the study of variable heating functions begins with these values. The energy budgets for experiments 3 through 6 are summarized in table 2 for comparison with later experiments.

B. RADIAL VARIATION OF LATENT HEATING

From the premise of the thermal forcing of the hurricane, differences between size and intensity of individual storms are related to space and time variations of the heating distributions. However, the question of just how sensitive or responsive is the storm circulation to these variations remains unanswered. In this subsection and the following one, the results of the model attained from various combinations of horizontal and vertical heating distributions provide some insight into this relation between the hurricane circulation and thermal forcing.

The heating function in experiment 6 (Anthes 1970*a*) produced a rather large storm of only moderate intensity. The total heat release, generation of available energy, and conversion to kinetic energy were larger than empirical results by a factor of 2 or 3. These results suggest that the heating function overestimates the latent heat release at large distances from the center.

In experiments 7 and 8, the latent heat release beyond 100 km is progressively decreased with the result that the heating becomes more concentrated near the center (rainfall types B and C in table 3 and fig. 3). In these experiments, the vertical heating distribution is specified by the solid curve in figure 4.

TABLE 2.—*Energy transformation rates* (10^{18} W)

Experiment	3	4	5	6	7	8	9	10	11	14
Rainfall profile type	A	A	A	A	B	C	B	0.5B	B	B
Vertical profile (p, pseudoadiabatic; c, cloud environment)	c	c	c	c	c	c	p	c	c	c
K_H (10^8 cm^2/s)	25.0	10.0	10.0	5.0	5.0	5.0	5.0	5.0	5.0	2.5
K_v (10^6 cm^2/s)	0.5	1.0	5.0	5.0	5.0	5.0	5.0	5.0	5.0	5.0
Generation A	24.1	21.2	15.5	17.3	10.7	4.8	2.9	13.7	13.8	9.9
Boundary A	18.2	17.0	13.3	14.6	4.2	0.1	1.1	5.0	2.4	3.5
Conversion to K	42.0	39.2	30.3	32.9	16.5	6.2	5.3	18.8	18.6	15.1
Boundary K	− 5.0	− 4.3	− 2.2	− 2.2	0.0	0.0	0.0	0.0	− 0.1	− 0.2
Drag dissipation	−18.0	−22.0	−15.0	−14.0	− 9.2	−7.0	−5.0	−11.0	− 9.4	−12.0
Lateral mixing	−26.0	−16.0	−12.0	− 6.8	− 5.7	−5.0	−3.0	− 5.8	− 5.9	− 4.2
Vertical mixing	− 2.5	− 6.0	−18.0	−15.0	−11.0	−5.0	−5.0	−10.0	−13.0	−13.0

TABLE 3.—*Summary of experiments investigating radial variation of heating*

Experiment	Rainfall type	Total heating rate 10^{14} W
6	A	21.3
7	B	11.0
8	C	5.5

Before the discussion of the steady-state solutions, quantitative results illustrating the convergence to a steady state as shown by the decrease of the L_2 norm are presented for a typical experiment. The behavior of L_2 in the other experiments is quite similar. In figure 6, the convergence of the tangential winds is most rapid in the lower levels near the center. Inside 200 km, the tangential wind has reached a slowly varying state after 800 iterations. In the upper levels, however, at large distances from the center, convergence is much slower. In fact, $L_2(v_\lambda)$ at 360°K does not begin to decrease until the inner region reaches a quasi-steady state (about 600 iterations). The tangential winds in the outer regions are primarily determined by the steady-state angular momentum distribution near the center. The slow convergence in this region reflects the time required for the angular momentum near the center to be advected to the edge of the domain.

The convergence of $L_2(v_\lambda)$ indicates that the solutions (for the 500-km domain) may approach arbitrarily close to a steady state, the only limit being the time (and cost) required for each experiment. However, the point of diminishing returns has probably been reached long before 6,400 steps, since the tangential wind components at selected points (fig. 6) are qualitatively in near-steady state after 1,600 iterations. For experiments with 20-km resolution, therefore, a compromise of 1,600 steps is considered adequate for meaningful comparisons between experiments.

The convergence of the L_2 norm on the radial winds for the surface and 360°K is shown in figure 7. The oscillations

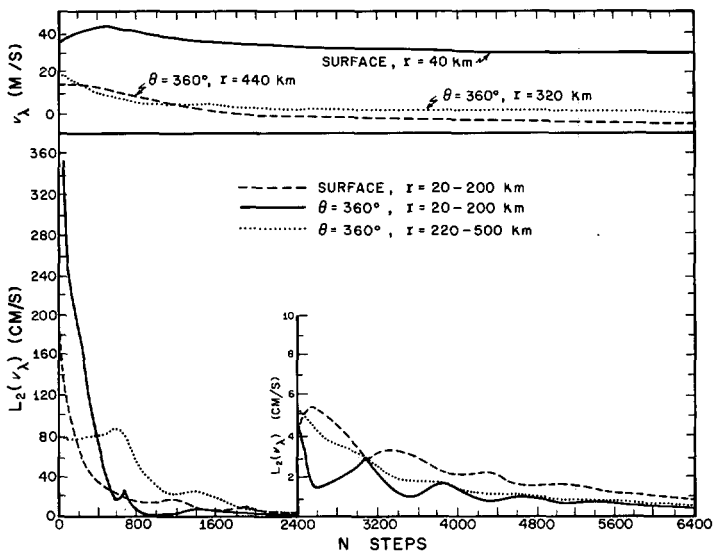

FIGURE 6.—Time (iteration step) variation of L_2 norm on tangential wind for the surface and 360°K in a typical experiment. Also shown is the variation of v_λ at three model points.

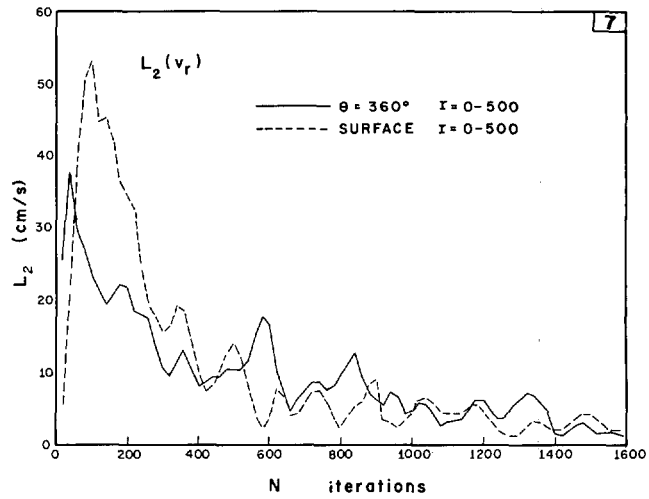

FIGURE 7.—Time (iteration step) variation of the L_2 norm on radial wind for the surface and 360°K in experiment 7.

TABLE 4.—*Empirical energy budgets*

Investigation	Region of storm	Heating	Generation of A	Conversion to K	Advection of K	Surface dissipation	Internal dissipation
	(km)	(10^{14} W)	(10^{12} W)	(10^{12} W)	(10^{12} W)	(10^{12} W)	(10^{12} W)
Anthes and Johnson (1968)	0–1000	3.2	10.3	—	—	—	—
Hawkins and Rubsam (1968)	0–150	2.2	—	2.3	3.9	−4.2	−2.0
Hughes (1952)	0–444	5.4	—	—	—	—	—
Miller (1962)	0–111	3.6	—	8.0	2.4	−5.1	−5.3
Palmén and Jordan (1955)	0–666	5.4	—	15.0	—	—	—
Palmén and Riehl (1957)	0–666	5.0	—	15.0	0.0	−13.0	0.0
Riehl and Malkus (1961)							
8/25	0–150	2.1	—	2.8	0.3	−1.6	−1.0
8/27	0–150	4.0	—	6.8	3.5	−3.2	−6.6

superimposed on the downward trend are evidence of inertial gravity waves.

Concentrated heating near the center, experiment 7. In this experiment (rainfall type B, fig. 3), the total heating rate is reduced from 21.3 to 11.0×10^{14} W, a rate closer to empirical results (table 4). The more concentrated heating function in this experiment generates a smaller warm core with nearly as intense a pressure gradient near the center as the one in experiment 6. The tangential and radial wind profiles are shown in figure 9 and may be compared with those from experiment 6 in figure 8. The effect of reducing the heating beyond 150 km on the tangential wind is to slightly decrease the maximum tangential wind from 34 to 33 m/s at 60 km. However, the winds beyond 150 km decrease significantly. The 3-percent decrease in the maximum tangential wind speed, despite a 50-percent reduction in total heating is somewhat paradoxical and emphasizes the importance of differential heating in establishing the temperature and pressure gradients and the angular momentum distribution.

The changes in the radial winds are greater than those in the tangential winds (figs. 8B and 9B). The inflow at the surface is reduced beyond 200 km (e.g., from 11 to 8 m/s at 250 km). The maximum outflow decreases from 19 to 14 m/s, and the radius of maximum outflow moves inward from 360 to 180 km.

The results from experiment 7 correspond to a minimal hurricane. The tangential winds show a region of maximum cyclonic winds near the center with little vertical wind shear below 300 mb. In the lower levels beyond the radius of maximum wind, positive vertical shear exists because of surface friction. A small region of anticyclonic winds occurs in the upper levels beyond 400 km.

The radial wind profiles show inflow from the surface to about 600 mb, although significant ($|v_r| \geq 5$ m/s) inflow is limited to the region below 800 mb. The maximum inflow of 15 m/s is somewhat stronger than empirical observations (e.g., Miller 1962) but weaker than the inflow found in separate boundary-layer experiments (Anthes 1970*a*). Significant outflow occurs above 300 mb.

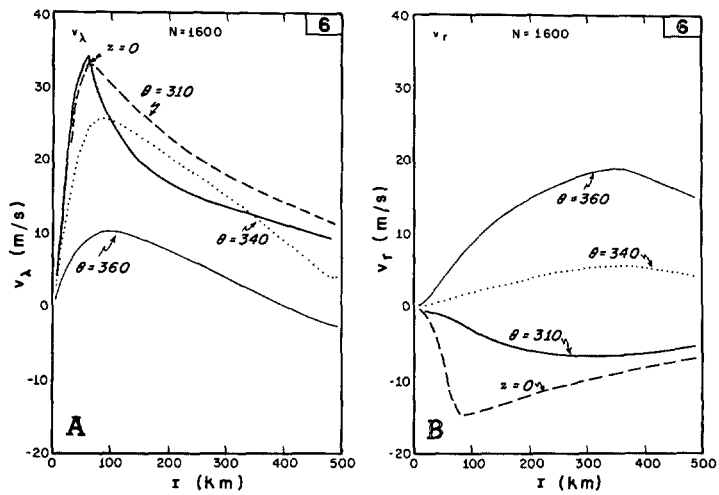

FIGURE 8.—Radial profiles of slowly varying (1,600 iterations) tangential (A) and radial (B) winds for various levels in experiment 6.

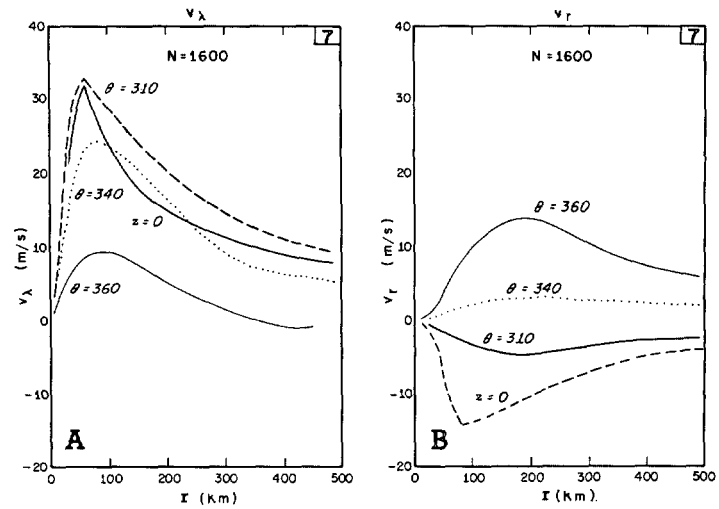

FIGURE 9.—Radial profiles of slowly varying (1,600 iterations) tangential (A) and radial (B) winds for various levels in experiment 7.

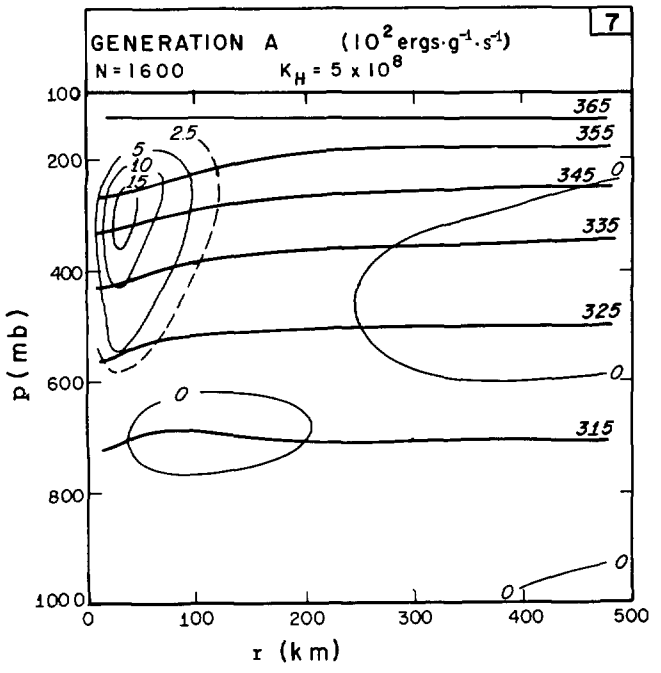

FIGURE 10.—Generation of available potential energy cross section for a slowly varying state (1,600 iterations) in experiment 7.

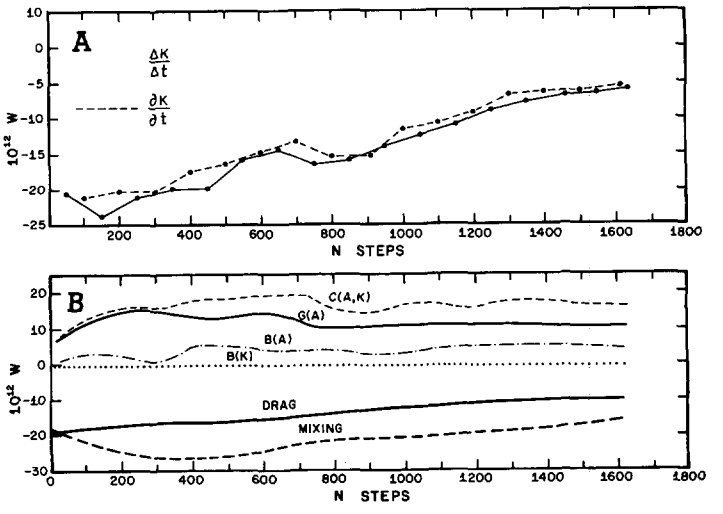

FIGURE 11.—(A) observed ($\Delta K/\Delta t$) and analytic ($\partial K/\partial t$) kinetic energy tendencies in experiment 7 and (B) time (iteration step) variation of energy budget components in experiment 7.

The vertical cross sections of the generation of available potential energy, A, are shown in figure 10. Most of the generation occurs in the middle and upper troposphere inside 150 km, a result that agrees well with the empirical estimate of Anthes and Johnson (1968). On the other hand, conversion of available to kinetic energy, C(A, K), occurs mainly below 800 mb inside 300 km where the inflow and acceleration toward lower pressure are large.

The difference between observed rates of change in the total kinetic energy of the volume and the instantaneous tendencies computed from eq (29) is an estimate of the truncation error in the model. The tendencies as a function of iteration step and the observed changes evaluated over 100 steps (fig. 11A) show little systematic deviation. Maximum differences are about 10 percent, indicating that truncation error is small.

Figure 11B shows the evolution of the different components of the rates of change of available potential and kinetic energy. Initially, the dissipation by horizontal mixing is dominant, causing a large negative kinetic energy tendency. The internal mixing decreases slowly after 400 steps. Throughout the entire experiment, the dissipation from surface drag is smaller than that from internal mixing.

One of the most interesting features of the energy budget evolution is the relationship between changes in the generation G(A) and boundary flux B(A) of available potential energy and its conversion to kinetic energy. Although energetic consistency requires only that these changes be equal in the steady state, there is an extremely close correlation between the two at all stages of all the experiments. This suggests that the available energy generated by the steady forcing is almost immediately converted to kinetic energy.

Initially, the kinetic energy conversion closely follows the generation. After 300 steps, however, the mass outflow is removing heat at 500 km that would otherwise reduce the radial temperature gradient. This process is reflected in an increase in the boundary term B, of the available energy change equation. The sum of the generation and boundary terms continues to almost exactly balance the conversion to kinetic energy, so that changes in the store of available potential energy are small.

Although the boundary term in the available energy budget is large, the boundary flux of kinetic energy B(K) is small compared to the conversion and dissipation processes within the volume. The contribution is relatively constant and is negative, indicating that the storm is exporting kinetic energy to the environment.

The contribution by the various energy transformation processes within 100-km radial rings is presented in figure 12. Most of the generation occurs inside 200 km while its conversion to kinetic energy occurs primarily between 100 and 300 km. The large contribution to the available energy budget by the boundary processes supports earlier studies which show that the hurricane cannot be considered a closed system on this scale. In the total energy budget (table 2), the generation of available potential energy and its conversion to kinetic energy are reduced to 10.7 and 16.5×10^{12} W, respectively—values that compare favorably with the empirical results in table 4. The kinetic energy sinks are 9.2×10^{12} W for surface drag, 11.0×10^{12} W for vertical (V) mixing, and 5.7×10^{12} W for horizontal (H) mixing. Comparison of these dissipation rates with empirical results is difficult. While the dissipation by drag friction is readily computed from hurricane wind data, dissipation by internal mixing is usually

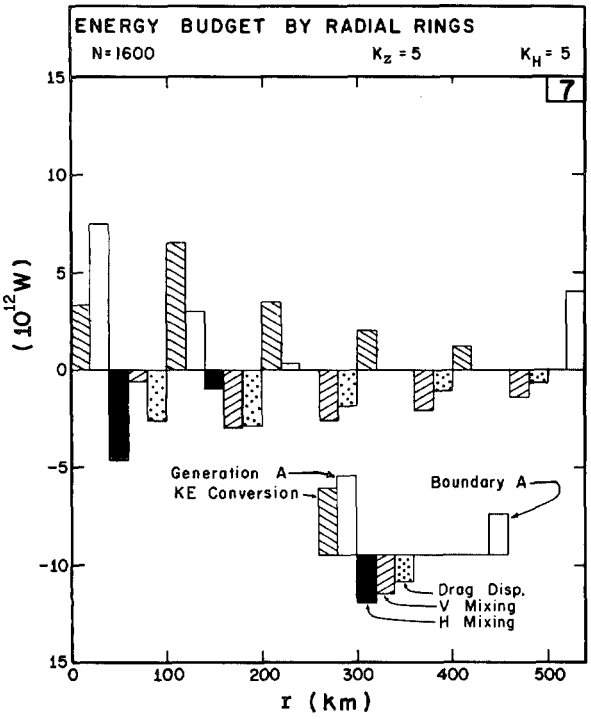

FIGURE 12.—Energy budget components within 100-km radial rings for a slowly varying state (1,600 iterations) in experiment 7.

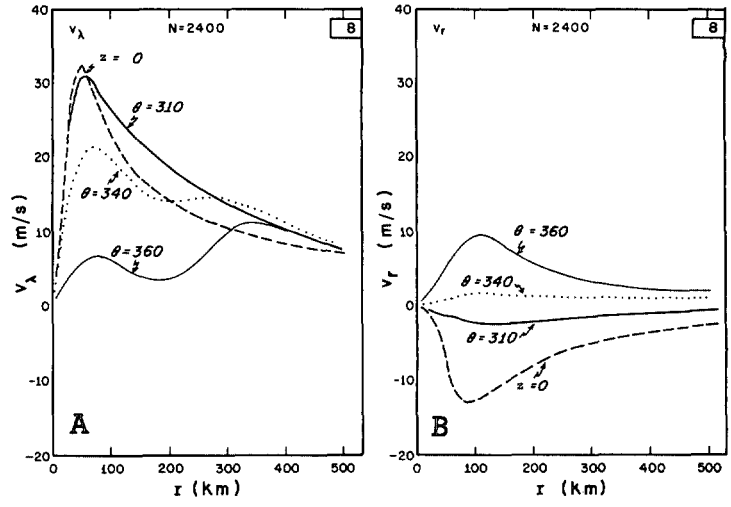

FIGURE 13.—Radial profiles of slowly varying (2,400 iterations) tangential (A) and radial (B) winds for various levels in experiment 8.

computed as a residual in a kinetic energy budget. Also, the empirical results in table 4 were determined for only a small portion of the storm ($r \leq 150$ km).

The ratio of internal mixing to surface friction in table 4 ranges from 0.48 to 2.06. The ratio in experiment 7 is 1.8 which is near the upper limit of the empirical estimates (the range of this ratio in all subsequent experiments is 1.02 to 2.01). Beyond 200 km, the vertical mixing may be overestimated for two reasons. First, the assumption that K_z is constant horizontally is very crude. The vertical turbulence, including cumulus convection, probably decreases with increasing radius; therefore, K_z in the model should decrease also. Second, the large vertical mixing dissipation is related to the fact that the middle-level winds in the outer region have not yet completely adjusted to the upper and lower level winds, a consequence of weak vertical coupling in the absence of heating. Thus, the vertical shear resulting from the initial conditions is still large.

In summary, the effect of reducing the heating beyond 200 km in experiment 7 is to significantly reduce the tangential and radial wind components at larger radii. For a reduction of the total heating by 50 percent, only a 3-percent decrease in maximum tangential wind is produced. The generation and conversion of available energy and dissipation of kinetic energy compare favorably with empirical evidence, even though the total heating is somewhat high.

Very concentrated heating near center, experiment 8. The thermal forcing by the extremely concentrated heating function, type C in figure 3, is studied in experiment 8. Inside 100 km, the horizontal distribution is essentially unchanged from that in experiments 6 and 7. The heating rate beyond 100 km is greatly reduced; and the total heating decreases to 5.5×10^{14} W, an amount comparable to observational evidence (table 4).

Because of the concentrated heating distribution, a variable grid was utilized in experiment 8. For $r \leq 160$ km, the resolution is 10 km. For $r > 160$ km, the resolution varies smoothly from 10 km to 25 km at the maximum radius of 500 km. The use of a variable grid is justified in a later experiment.

Within 100 km, the tangential and radial wind profiles for experiment 8 (fig. 13) are quite similar to the profiles for experiment 7 (fig. 9). The slight shift inward of the maximum wind from 60 km (exp. 7) to 50 km (exp. 8) is probably a consequence of the increased resolution rather than the heating reduction beyond 100 km.

Although changes inside 100 km are small, large differences are present at greater distances. Maximum outflow is reduced from 14 m/s at 180 km (exp. 7) to 10 m/s at 100 km (exp. 8). At 300 km, the outflow is reduced from 11 m/s to 3 m/s.

The decreased outflow produces a different tangential wind distribution at larger radii. Whereas the stronger outflow in experiments 6 and 7 produces anticyclonic winds at 500 km by an outward advection of low angular momentum from the center, there is little radial advection at this distance in experiment 8. Thus internal mixing dominates, and the tangential winds slowly decay.

The energy budget reflects the decrease in storm intensity compared with experiments 6 and 7. The generation of available energy occurs entirely within 100 km. The boundary term in the available energy budget decreases from 4.2×10^{12} to 0.1×10^{12} W. The total

energy budget (table 2) shows significantly smaller values for all processes, except horizontal mixing.

Experiments 6, 7, and 8 indicate that the reduction of heating at large distances has little effect on the inner region of the storm and suggests that the maximum winds are determined primarily by heating in the inner region. As the heating is reduced at larger distances, the storm decreases in horizontal extent; and the tangential and radial winds beyond 100 km are reduced. The size and intensity of the anticyclone aloft are closely related to the amount of heating at large distances from the center. This relationship suggests that the intensity of the thermal anticyclone associated with storms in nature should be closely correlated with the diameter of the active convective area.

C. VERTICAL VARIATION OF LATENT HEATING, EXPERIMENT 9

The vertical distribution of latent heating is an important aspect of the tropical cyclone problem. Early attempts at hurricane modeling (e.g., Kasahara 1961 and Rosenthal 1964) related the heating to the variation of saturation specific humidity, q_s, along an appropriate moist adiabat. This pseudoadiabatic type of heating resulted in unrealistic circulations and showed that the hurricane could not be considered a huge cloud. Kuo (1965) attempted to relate the large-scale to the cloud scale heating by making the heat release at any level proportional to the cloud-environment temperature difference. Parameterization similar to this type of heating (hereafter called "cloud-environment" type) has given quite realistic results in hurricane models (Yamasaki 1968*a*, 1968*b*; and Rosenthal 1969).

In experiment 9, the vertical distribution of heating is proportional to $\partial q_s/\partial p$ along the moist adiabat defined by an equivalent potential temperature of 365°K. The relative distribution is contrasted with the vertical heating distribution of the earlier experiments in figure 4. The horizontal heating distribution and all other parameters are identical to those in experiment 7.

Figure 14 shows the radial profiles of tangential and radial winds in experiment 9. The low-level tangential wind profiles are similar to those in experiment 7 (fig. 9). The reduced vertical transport of momentum in the upper levels, however, yields weaker winds. The radial wind profiles show a deep, weak outflow layer in experiment 9 in contrast to the shallow, stong outflow layer of experiment 7. This difference is related to the change in thermal structure shown in figure 15. In experiment 9, the level of maximum temperature departure drops from 300 to 500 mb, the pressure gradient decreases more rapidly with height, and the outflow begins at lower levels. Near 200 mb, the atmosphere is nearly undisturbed.

The upper level temperature structure and the radial winds of experiment 9 are not supported by empirical evidence. Observations show that the maximum temperature departure occurs in the upper rather than middle troposphere (Hawkins and Rubsam 1968 and Malkus and Riehl 1961). They also support a thin, strong outflow

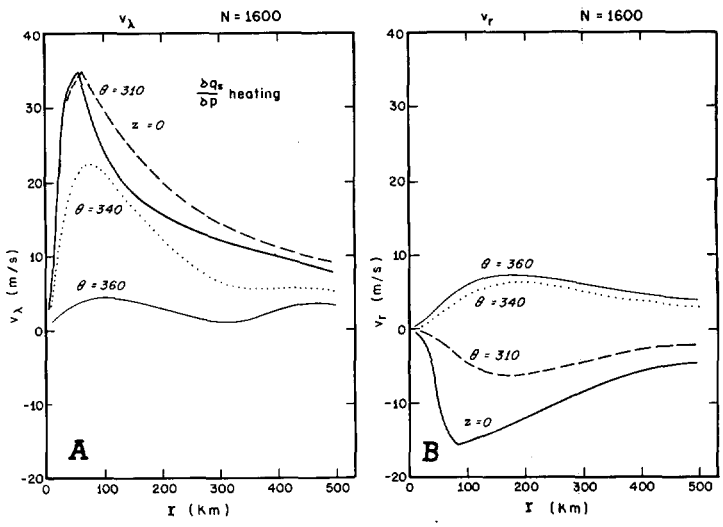

FIGURE 14.—Radial profiles of slowly varying (1,600 iterations) tangential (A) and radial (B) winds for various levels in experiment 9.

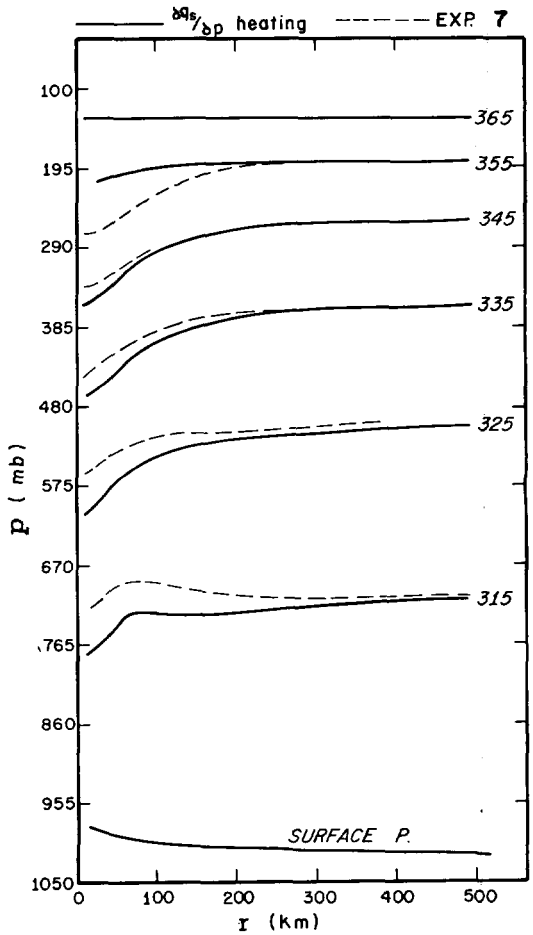

FIGURE 15.—Isentropic cross section for slowly varying state (1,600 iterations) in experiments 7 and 9.

layer rather than a deep, sluggish layer (Miller 1958, 1964). These results confirm that the vertical heating distribution of experiment 9 is not appropriate to the hurricane scale in the mature, slowly varying state.

D. VARIATION OF TOTAL HEATING, EXPERIMENT 10

The results from the previous experiments emphasize the importance of variable heating distributions. In all the experiments, the heating maximum was defined by a rainfall rate of about 50 cm/day at 30 km, a moderate rate for a mature hurricane. In experiment 10, the heating function is one-half that of experiment 7, while the horizontal and vertical heating variation and all other parameters are identical.

As expected, the tangential and radial circulations are considerably less than those in experiment 7; and the thermal structure shows a weaker warm core. The maximum tangential wind is reduced from 33 to 25 m/s; maximum inflow is reduced from 15 to 9 m/s, while the outflow is decreased from 14 to 7 m/s. The maximum temperature departure is reduced from +10° to +4°C. The profiles are not shown. Thus, the thermal forcing given by the rainfall rates of experiment 10 produces maximum winds that are typical of a weak tropical storm.

E. EXPERIMENTS OF A COMPUTATIONAL NATURE

The experiments so far have emphasized primarily the role of physical processes such as variable mixing and heating in the determination of steady circulations. In numerical models, however, it is also important to ascertain the effect of the computational or artifical aspects of the model on the solutions. Ideally, the effects of domain size, boundary conditions, and resolution should be small in comparison to physical effects. The experiments in this section compare solutions with domains of 500 and 1000 km, with constant horizontal resolutions of 10 and 20 km, and with a variable horizontal grid.

Domain size, experiment 11. The effect of the arbitrary horizontal boundary conditions may be investigated by increasing the size of the horizontal domain. Experiments 7 and 11 are identical, except that the horizontal domain of 500 km is extended to 1000 km in the latter. Figure 16 shows the tangential wind profiles for both experiments. Differences for $r<200$ km are less than 30 cm/s at all levels. Between 300 and 500 km, however, the maximum difference is 1 m/s. The low-level tangential winds show greater anticyclonic shear in experiment 11, a result of the boundary condition of zero relative vorticity being shifted from 500 km in experiment 7 to 1000 km in experiment 11.

A small difference is also present in the low-level radial wind profile (not shown). The boundary condition of zero divergence at 500 km in experiment 7 is replaced by weak positive divergence in experiment 11, and the inflow is less by 0.4 m/s at this distance. The small differences between these two experiments, especially near the radius of maximum winds, justify the use of the 500-km domain.

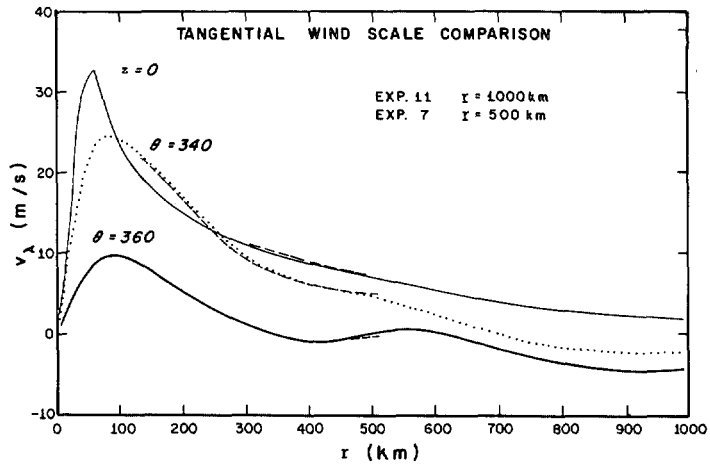

FIGURE 16.—Radial profile of slowly varying (1,600 iterations) tangential winds at various levels in experiments 7 and 11.

Variable grid, experiment 12. In numerical models of atmospheric convective phenomena such as cumulus clouds, squall lines, or hurricanes, a greater resolution for a portion of the domain is desirable. For the hurricane, a finer mesh is needed near the eye wall where horizontal gradients are larger than in the environment of the storm where gradients are weak. The variable grid for this model is defined by retaining a constant grid from the origin to R_0 and introducing the transformation $r=R_0+x^2+cx$ for $r>R_0$. This transformation, with proper choice of R_0, c, and increment, Δx, increases computing efficiency with no significant reduction in accuracy.

Results from a variable and a fixed grid are compared, where the size of the domain is 1000 km and the horizontal resolution for $r\leq 300$ km is 20 km in both experiments. For the variable grid (exp. 12), the parameters of the transformation are $R_0=300$ km, $c=395.1$ m$^{1/2}$, and $\Delta x=43.6$ m$^{1/2}$. The resolution varies from 20 km at 300 km to 73.3 km at 1000 km. The number of grid points is reduced from 51 to 31, and a 40-percent saving in the computational time is achieved. Initial conditions for the grid points beyond 300 km are interpolated from the profiles of the fixed grid.

Figure 17 shows the radial wind profiles after 1,600 iterations. Differences are extremely small; for example, the difference in maximum inflow between the variable grid experiment and the fixed grid experiment is 0.09 m/s. The maximum tangential wind difference is 0.05 m/s. Exact comparisons beyond 300 km are difficult because the grid points in the two experiments do not coincide. Qualitatively, however, the results agree very well and suggest that a further reduction in grid points may be possible without generating unacceptable errors. The close agreement between experiments 11 and 12 justifies use of the variable grid as an economically useful substitute for the constant grid.

High (10-km) resolution, experiment 13. In the final experiment of a computational nature, experiment 7 is

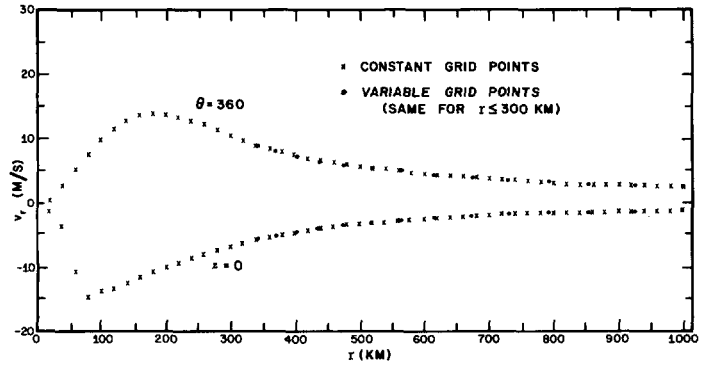

FIGURE 17.—Radial profile of radial winds after 1,600 iterations in experiments 11 and 12.

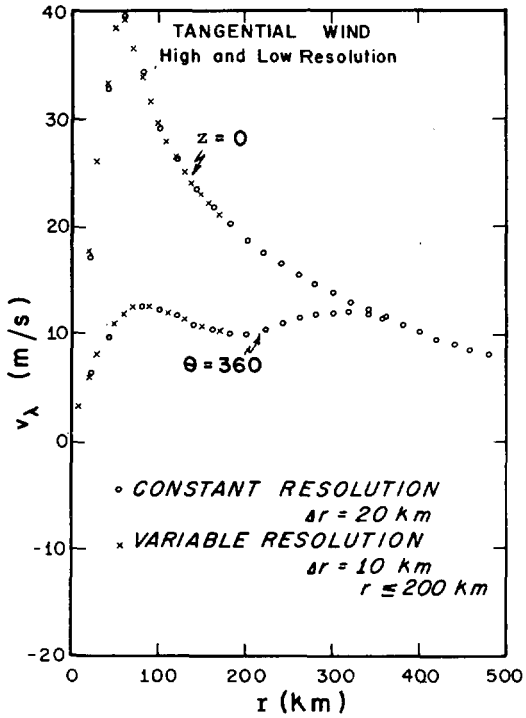

FIGURE 18.—Radial profile of tangential winds after 400 iterations in experiment 7 and 800 iterations in experiment 13.

repeated utilizing the variable grid. For $R_0=150$ km, $c=484.1$ m$^{1/2}$, and $\Delta x=19.85$ m$^{1/2}$, the resolution varies from 10 km within 150 km of the center to 25 km at the outer boundary of 500 km. The number of grid points increases from 26 in experiment 7 to 36 in experiment 13. Because the time step must be halved to satisfy the linear computational stability requirement, an increase in computation time of 138 percent is required.

Figure 18 shows the tangential wind profiles for 400 and 800 iterations, respectively. The profiles for experiment 13 are somewhat smoother near the radius of maximum wind than for experiment 7. The maximum tangential wind is

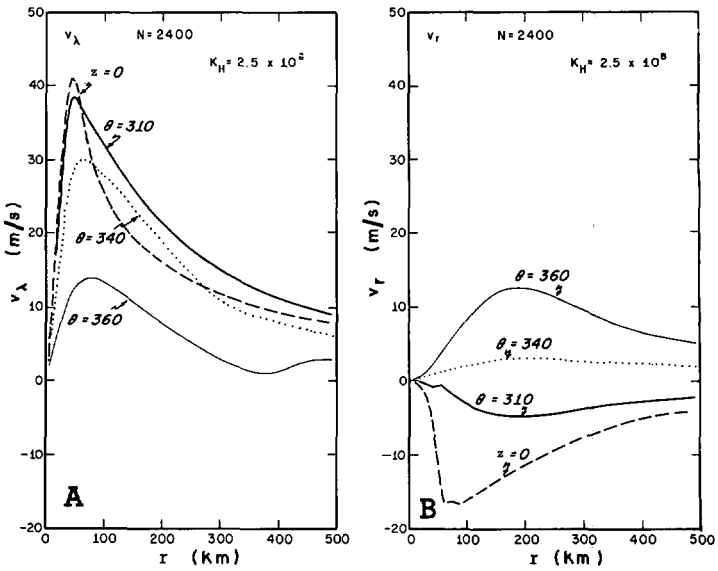

FIGURE 19.—Radial profile of slowly varying (2,400 iterations) tangential (A) and radial (B) winds for various levels in experiment 14.

reduced from 39.28 in experiment 7 to 38.65 m/s in experiment 13, while the maximum inflow decreases from 18.28 to 17.63 m/s. These differences, which are about 2 percent, appear insignificant in view of the 138-percent increase in computational time.

F. HIGH-RESOLUTION EXPERIMENT WITH REDUCED HORIZONTAL MIXING, EXPERIMENT 14

After the preliminary series of experiments, a value for K_H of 5×10^8 cm^2/s was used in subsequent experiments. For investigating the effect of decreasing this horizontal mixing coefficient to 2.5×10^8 cm^2/s, the variable grid of experiment 13 with 10-km resolution near the center and the heating function of experiment 7 is utilized.

Momentum and temperature structures. Figure 19 shows the slowly varying tangential and radial wind profiles for experiment 14 which should be compared to those for experiment 7 (fig. 9). The maximum tangential wind increases from 33 to 41 m/s in experiment 14, and the radius of maximum wind shifts inward from 60 to 40 km. Maximum inflow increases from 15 to 17 m/s. The irregularity in the radial wind profile at 70 km indicates that the resolution in this region is insufficient to adequately resolve the extremum. The temperature structure shows a more concentrated warm core in experiment 14 than in experiment 7, with a maximum temperature anomaly increase of 3°C.

The circulation in experiment 14 is the strongest of all the experiments. Figures 20 and 21 show cross sections of the tangential and radial wind. The tangential circulation is stronger and more concentrated near the center than in experiment 7. The weak upper level anticyclone at 500 km in experiment 7 is not present because the cyclonic circulation in the upper levels near the center is stronger

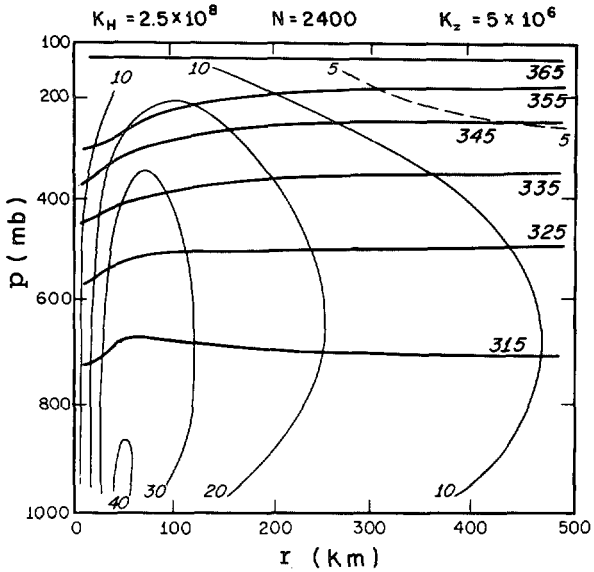

FIGURE 20.—Tangential wind (m/s) cross section for the slowly varying state (2,400 iterations) in experiment 14.

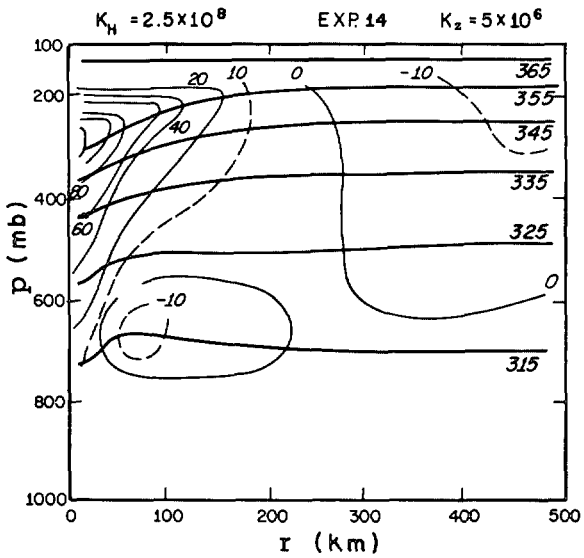

FIGURE 22.—Efficiency factor (10^{-3}) cross section for the slowly varying state (2,400 iterations) in experiment 14.

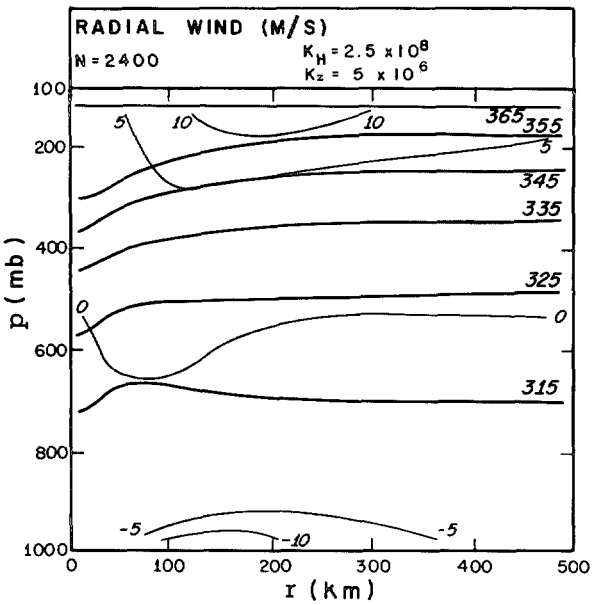

FIGURE 21.—Radial wind cross section for the slowly varying state (2,400 iterations) in experiment 14.

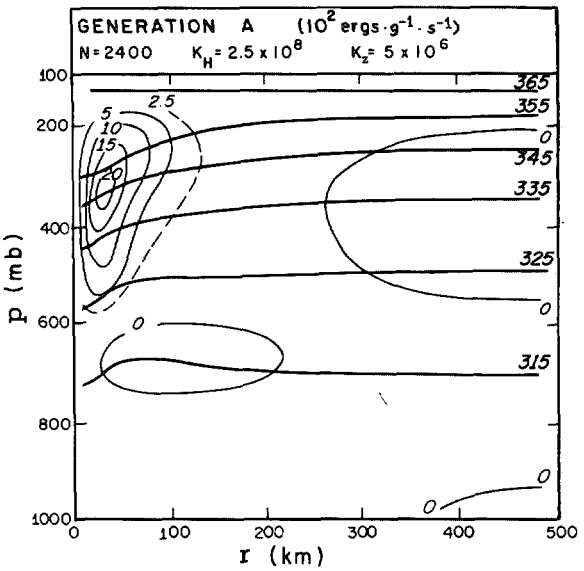

FIGURE 23.—Generation of available potential energy cross section for the slowly varying state (2,400 iterations) in experiment 14.

in experiment 14, so that the radius at which the relative circulation becomes anticyclonic is greater. This result and the strong dependency of the upper level outflow on the horizontal heating distribution found earlier suggest that relatively weak storms with large diameters should be accompanied by stronger upper level anticyclones than smaller more intense storms.

Energy budget. The efficiency factor cross section for experiment 14 (fig. 22) shows positive efficiency factors in the middle and upper troposphere extending from the center to 300 km. Negative efficiency factors occur in the lower levels near the center and in the upper levels beyond 300 km. In figure 23, almost all the generation occurs inside 200 km and above 600 mb.

The energy budget shown in figure 24 and the total budget summarized in table 2 are quite similar to the results from experiment 7 (fig. 12). Although the dissipation of kinetic energy by horizontal mixing is reduced in experiment 14, the dissipation at the surface and through vertical mixing is increased. The latter increases are due to the greater low-level wind speed and the increased vertical wind shear.

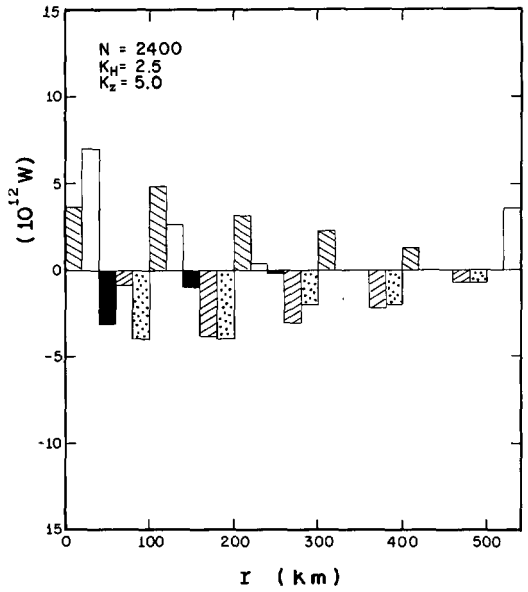

FIGURE 24.—Energy budget components within the 100-km radial rings for the slowly varying state (2,400 iterations) in experiment 14 (see fig. 12 for the key).

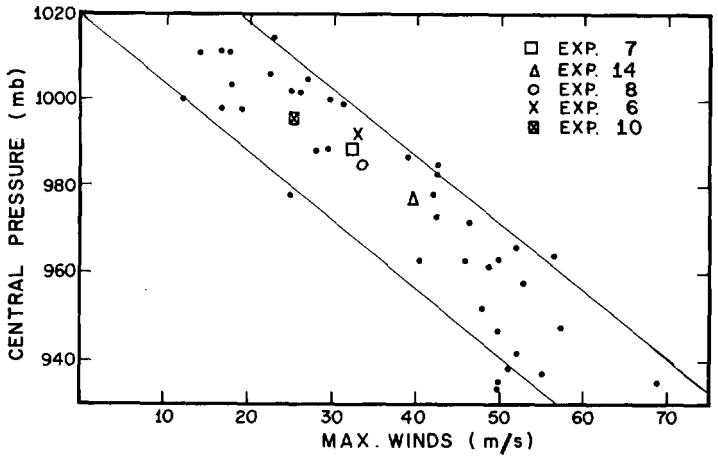

FIGURE 25.—Scatter diagram of maximum surface winds versus central pressure for empirical data (Colón 1963) and model experiments.

G. NUMERICAL AND EMPIRICAL PRESSURE-WIND RELATIONSHIP

Empirical evidence (Colón 1963) indicates a close relationship between central pressure and maximum wind speed. Figure 25 shows the model results from five experiments superimposed on Colón's data. Central pressure in the model is defined as the pressure at the first prediction point for pressure, which is either 5 or 10 km. All points from the model experiments lie within a region that bounds the empirical data.

The relationship between central pressure and radius of maximum wind is another aspect of the model to be

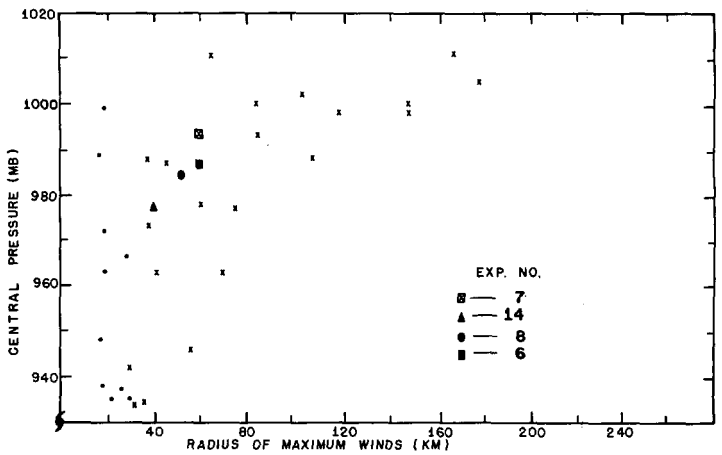

FIGURE 26.—Scatter diagram of radius of maximum surface winds versus central pressure for empirical data (Colón 1963) and model experiments.

compared with Colón's (1963) data (fig. 26). Colón discusses two types of storms. The "Daisy type," represented by dots in figure 26, is small and shows little relationship between central pressure and radius of maximum wind. The "Helene type" storm, represented by crosses in figure 26, is larger and shows an increasing radius of maximum wind with increasing central pressure. From figure 26, we see that storms produced by this model appear to fit the Helene type.

The degree of gradient balance throughout the storm system has received attention from investigators (e.g., Hawkins and Rubsam 1968). Their results show that the inner region is fairly close to gradient balance. In these experiments, except for the winds near the surface which are subgradient by 20 to 40 percent and in the outflow layer where radial advection is important, gradient balance is closely approximated. Models with low vertical resolution may have outflow layers closer to gradient balance because horizontal advection in a deeper outflow layer will be much weaker.

5. SUMMARY

A diagnostic model in isentropic coordinates is developed to study the energetics and dynamics of the steady-state mature tropical cyclone. Slowly varying solutions for the mass and momentum fields are obtained by an iterative technique for the thermal forcing specified by several heating distributions. The principle conclusions from the preliminary experiments are:

1. The magnitude and distance of the maximum wind from the center is determined primarily by the heating inside 100 km. Large variations in heating beyond 100 km have little effect on the maximum wind but produce considerable changes in the outflow intensity. Because angular momentum tends to be conserved in the outflow layer, the size and intensity of the upper level anticyclone is also closely related to the heating at large distances from the center.

2. In experiments in which the vertical variation of heating is proportional to the condensation of water vapor along a moist adiabat, the temperature structure shows a low-level warm core and a deep, weak outflow layer. A vertical distribution that releases a higher proportion of heat in the upper troposphere gives more realistic results.

3. In experiments with a constant horizontal eddy coefficient and a vertical mixing coefficient that decreases linearly with height, values of $K_H > 5\times10^8$ cm^2/s result in diffuse storms; and values of $K_z < 1\times10^6$ cm^2/s produce storms with large vertical shear. Results most similar to observations are obtained for $K_H = 2.5$ and 5×10^8 cm^2/s and $K_z = 5\times10^6$ cm^2/s.

4. In the slowly varying states, the generation and boundary flux of available potential energy, conversion to kinetic energy, and dissipation of kinetic energy by surface and internal friction are balanced. Paradoxically, therefore, experiments with the most internal friction contain the most kinetic energy. The relationship between low-level inflow, high-level outflow, and the warm core structure produce a positive boundary contribution to the available potential energy budget. On a scale of 500 km, this boundary term is nearly as large as the generation term in some experiments. On a scale of 1000 km, however, the generation is an order of magnitude greater.

5. In the computational experiments, it is established that a 500-km domain and 20-km resolution are satisfactory for the latent heating functions studied. A variable grid is utilized in some experiments to economically gain higher resolution near the center. For a 40-percent gain in computational time, differences in maximum wind are less than 0.1 percent using the variable grid.

6. Isentropic coordinates may be used effectively in numerical models and are particularly effective in studying adiabatic and diabatic effects.

Although the results presented have shown that the size and intensity of the tropical cyclone is directly linked to thermal forcing, the question of what determines the heating profiles has not been investigated. Large-scale synoptic features such as sea and environment temperatures and horizontal and vertical shears are all important in determining the distribution of convection that leads to the development and maintenance of the tropical storm. Theoretical investigation of these properties will require more sophisticated numerical models to describe the delicate balance in the early stages of hurricane development.

ACKNOWLEDGMENTS

This work is part of a doctorate thesis from The University of Wisconsin. The author extends his sincere thanks to his advisor, Dr. Donald R. Johnson, for his continuing interest, helpful suggestions, and many profitable discussions throughout the course of this research.

The author also wishes to thank Dr. Stanley L. Rosenthal, National Hurricane Research Laboratory (NHRL), for his many helpful ideas at various stages of this research and Dr. R. Cecil Gentry, Director of NHRL, for the opportunity to work at NHRL and use its computing facilities.

Thanks are also due the author's reading committee, Profs. Werner Schwerdtfeger and John Young, for their helpful suggestions.

REFERENCES

Anthes, Richard A., "A Diagnostic Model of the Tropical Cyclone in Isentropic Coordinates," *ESSA Technical Memorandum* ERLTM–NHRL 89, U.S. Department of Commerce, National Hurricane Research Laboratory, Miami, Fla., Apr. **1970***a*, 147 pp.

Anthes, Richard A., "The Role of Large-Scale Asymmetries and Internal Mixing in Computing Meridional Circulations Associated With the Steady-State Hurricane," *Monthly Weather Review*, Vol. 98, No. 7, July **1970***b*, pp. 521–528.

Anthes, Richard A., and Johnson, Donald R., "Generation of Available Potential Energy in Hurricane Hilda (1964)," *Monthly Weather Review*, Vol. 96, No. 5, May **1968**, pp. 291–302.

Barrientos, Celso S., "Computations of Transverse Circulation in a Steady State, Symmetric Hurricane," *Journal of Applied Meteorology*, Vol. 3, No. 6, Dec. **1964**. pp. 685–692.

Colón, José A., "On the Evolution of the Wind Field During the Life Cycle of Tropical Cyclones," *National Hurricane Research Project Report* No. 65, U.S. Department of Commerce, Weather Bureau, Miami, Fla., Nov. **1963**, 36 pp.

Dutton, John A., and Johnson, Donald R., "The Theory of Available Potential Energy and a Variational Approach to Atmospheric Energetics," *Advances in Geophysics*, Vol. 12, **1967**, pp. 333–436.

Eliassen, Arnt, and Raustein, Elmer, "A Numerical Integration Experiment With a Model Atmosphere Based on Isentropic Surfaces," *Meteorologiske Annaler*, Vol. 5, No. 2, Oslo, Norway, **1968**, pp. 45–63.

Estoque, Mariano A., and Fernandez-Partagas, José J., "Hurricane Studies: Part II," *Institute of Atmospheric Science Paper* No. 2, University of Miami, Coral Gables, Fla., Mar. **1968**, pp. 28–65.

Gray, William M., "The Mutual Variation of Wind, Shear, and Baroclinicity in the Cumulus Convective Atmosphere of the Hurricane," *Monthly Weather Review*, Vol. 95, No. 2, Feb. **1967**, pp. 55–73.

Hawkins, Harry F., "Vertical Wind Profiles in Hurricanes," *National Hurricane Research Project Report* No. 55, U.S. Department of Commerce, Weather Bureau, Miami, Fla., June **1962**, 16 pp.

Hawkins, Harry F., and Rubsam, Daryl T., "Hurricane Hilda, 1964: I. Genesis, as Revealed by Satellite Photographs, Conventional and Aircraft Data," *Monthly Weather Review*, Vol. 93, No. 7, July **1968**, pp. 428–452.

Hughes, Lawrence A., "On the Low-Level Wind Structure of Tropical Storms," *Journal of Meteorology*, Vol. 9, No. 6, Dec. **1952**, pp. 422–428.

Johnson, Donald R., "The Available Potential Energy of Storms," *Journal of the Atmospheric Sciences*, Vol. 27, No. 5, Aug. **1970**, pp. 727–741.

Johnson, Donald R., and Dutton, John A., "Atmospheric Energetics and the General Circulation Viewed From Isentropic Coordinates," paper presented at the Conference on the Global Circulation of the Atmosphere, London, England, Aug. 25–29, **1969**.

Jordan, Charles L., "Mean Soundings for the West Indies Area," *Journal of Meteorology*, Vol. 15, No. 1, Feb. **1958**, pp. 91–97.

Kasahara, Akira, "A Numerical Experiment on the Development of a Tropical Cyclone," *Journal of Meteorology*, Vol. 18, No. 3, June **1961**, pp. 259–282.

Krishnamurti, T. N., "On the Vertical Velocity Field in a Steady, Symmetric Hurricane," *Tellus*, Vol. 13, No.2, Stockholm, Sweden, May **1961**, pp. 171–180.

Kuo, Hsiao-Lan, "On Formation and Intensification of Tropical Cyclones Through Latent Heat Release by Cumulus Convection," *Journal of the Atmospheric Sciences*, Vol. 22, No. 1, Jan. **1965**, pp. 40–63.

LaSeur, Noel E., and Hawkins, Harry F., "An Analysis of Hurricane Cleo (1958) Based on Data From Research Reconaissance Aircraft," *Monthly Weather Review*, Vol. 91, Nos. 10–12, Oct.–Dec. **1963**, pp. 694–709.

Lorenz, Edward N., "Available Potential Energy and the Maintenance of the General Circulation," *Tellus*, Vol. 7, No. 2, Stockholm, Sweden, May **1955**, pp. 157–167.

Malkus, Joanne S., and Riehl, Herbert, "On the Dynamics and Energy Transformations in Steady-State Hurricanes," *Tellus*, Vol. 12, No. 1, Stockholm, Sweden, Feb. **1960**, pp. 1–20.

Margules, Max, "Über die Energie der Stürme" (On the Energy of Storms), *Jahrbuch Zentralamt für Meteorologie und Geodynamik*, Vol. 40, Austria, **1905**, 26 pp.

Matsuno, Taroh, "Numerical Integrations of the Primitive Equations by a Simulated Backward Difference Method," *Journal of the Meteorological Society of Japan*, Ser. 2, Vol. 44, No. 1, Tokyo, Feb. **1966**, pp. 76–84.

Miller, Banner I., "On the Maximum Intensity of Hurricanes," *Journal of Meteorology*, Vol. 15, No. 2, Apr. **1958**, pp. 184–195.

Miller, Banner I., "On the Momentum and Energy Balance of Hurricane Helene (1958)," *National Hurricane Research Project Report* No. 53, U.S. Department of Commerce, Weather Bureau, Miami, Fla., Apr. **1962**, 19 pp.

Miller, Banner I., "A Study of the Filling of Hurricane Donna (1960) Over Land," *Monthly Weather Review*, Vol. 92, No. 9, Sept. **1964**, pp. 389–406.

Ooyama, Katsuyuki, "Numerical Simulation of the Life-Cycle of Tropical Cyclones," *Journal of the Atmospheric Sciences*, Vol. 26, No. 1, Jan. **1969**, pp. 3–40.

Palmén, Erik H., "On the Formation and Structure of Tropical Hurricanes," *Geophysica*, Vol. 3, Helsinki, Finland, **1948**, pp. 26–38.

Palmén, Erik H., and Jordan, Charles L., "Note on the Release of Kinetic Energy in Tropical Cyclones," *Tellus*, Vol. 7, No. 2, Stockholm, Sweden, May **1955**, pp. 186–188.

Palmén, Erik H., and Riehl, Herbert, "Budget of Angular Momentum and Kinetic Energy in Tropical Cyclones," *Journal of Meteorology*, Vol. 14, No. 2, Apr. **1957**, pp. 150–159.

Riehl, Herbert, and Malkus, Joanne S., "Some Aspects of Hurricane Daisy, 1958," *Tellus*, Vol. 13, No. 2, Stockholm, Sweden, May **1961**, pp. 181–213.

Rosenthal, Stanley L., "Some Attempts to Simulate the Development of Tropical Cyclones by Numerical Methods," *Monthly Weather Review*, Vol. 92, No. 1, Jan. **1964**, pp. 1–21.

Rosenthal, Stanley L., "Numerical Experiments With a Multilevel Primitive Equation Model Designed to Simulate the Development of Tropical Cyclones. Experiment I," *ESSA Technical Memorandum* ERLTM-NHRL 82, U.S. Department of Commerce, National Hurricane Research Laboratory, Miami, Fla., Jan. **1969**, 36 pp.

Yamasaki, Masanori, "A Tropical Cyclone Model With Parameterized Vertical Partition of Released Latent Heat," *Journal of the Meteorological Society of Japan*, Vol. 46, No. 3, Tokyo, June **1968***a*, pp. 202–214.

Yamasaki, Masanori, "Detailed Analysis of a Tropical Cyclone Simulated With a 13-Layer Model," *Papers in Meteorology and Geophysics*, Vol. 19, No. 4, Tokyo, Japan, Dec. **1968***b*, pp. 559–585.

Yanai, Michio, "Formation of Tropical Cyclones," *Reviews of Geophysics*, Vol. 2, No. 2, May **1964**, pp. 367–414.

[*Received August 19, 1970; revised January 22, 1971*]